
ANOMALYMATCH: DISCOVERING RARE OBJECTS OF INTEREST WITH SEMI-SUPERVISED AND ACTIVE LEARNING

Pablo Gómez

European Space Agency (ESA)
European Space Astronomy Centre (ESAC)
Camino Bajo del Castillo s/n
28692 Villanueva de la Cañada
Madrid, Spain
pablo.gomez@esa.int

David O’Ryan

European Space Agency (ESA)
European Space Astronomy Centre (ESAC)
Camino Bajo del Castillo s/n
28692 Villanueva de la Cañada
Madrid, Spain
david.oryan@esa.int

May 8, 2025

ABSTRACT

Anomaly detection in large datasets is essential in fields such as astronomy and computer vision; however, supervised methods typically require extensive anomaly labelling, which is often impractical. We present AnomalyMatch, an anomaly detection framework combining the semi-supervised FixMatch algorithm using EfficientNet classifiers with active learning. By treating anomaly detection as a semi-supervised binary classification problem, we efficiently utilise limited labelled and abundant unlabelled images. We allow iterative model refinement in a user interface for expert verification of high-confidence anomalies and correction of false positives. Built for astronomical data, AnomalyMatch generalises readily to other domains facing similar data challenges. Evaluations on the GalaxyMNIST astronomical dataset and the miniImageNet natural-image benchmark under severe class imbalance (1% anomalies for miniImageNet) display strong performance: starting from five to ten labelled anomalies and after three active learning cycles, we achieve an average AUROC of 0.95 (miniImageNet) and 0.86 (GalaxyMNIST), with respective AUPRC of 0.77 and 0.71. After active learning cycles, anomalies are ranked with 71% (miniImageNet) to 93% precision in the 1% of the highest-ranked images. AnomalyMatch is tailored for large-scale applications, efficiently processing predictions for ≈ 100 million images within three days on a single GPU. Integrated into ESA’s Datalabs platform, AnomalyMatch facilitates targeted discovery of scientifically valuable anomalies in vast astronomical datasets. Our results underscore the exceptional utility and scalability of this approach for anomaly discovery, highlighting the value of specialised approaches for domains characterised by severe label scarcity.

Keywords Semi-supervised learning · Active learning · Anomaly detection · High-performance computing

1 Introduction

Identifying anomalies – rare and unusual outliers – in large datasets is a central challenge across machine learning and applied sciences [1, 2]. Anomalies often hold critical relevance, either as scientifically significant discoveries or as artefacts requiring removal.

There are various anomaly detection approaches, but they generally fall into three categories based on availability of labelled, i.e. known, anomalies: fully supervised, semi-supervised, and unsupervised methods. Fully supervised anomaly detection typically achieves the best performance but demands substantial labelled anomaly examples, which are often unavailable or prohibitively expensive to obtain [3]. Conversely, purely unsupervised methods operate without labels but can struggle to discriminate scientifically meaningful anomalies from irrelevant outliers or noise and do not easily allow to make use of known information and anomalies [4]. Semi-supervised learning (SSL) approaches,

which use unlabelled data along with some limited labelled instances, offer a practical balance, leveraging minimal supervision to improve performance significantly over fully unsupervised approaches [3, 5].

Real-world anomaly detection workflows often benefit from directly incorporating human expertise via active learning and user-in-the-loop approaches [6]. These frameworks allow iterative model refinement through user interaction, crucially exploiting expert domain knowledge to identify the most valuable anomalies from a scientific perspective. The *Astronomy* tool [7] is a prominent example in astronomy, effectively combining active learning with anomaly detection to iteratively refine its predictions based on user feedback. Additionally, citizen science projects such as Galaxy Zoo [8] have demonstrated the potential for non-expert volunteers to accelerate and scale the labelling process. Our work embraces this philosophy, emphasizing active learning to guide the anomaly detection pipeline toward scientifically interesting anomalies, rather than merely statistically unusual ones.

In this work, we introduce *AnomalyMatch*, a semi-supervised anomaly detection tool that integrates *FixMatch* [5] with an EfficientNet-based neural architecture [9], active learning, and a custom graphical user interface (GUI). This setup is then optimised for anomaly detection as a heavily imbalanced binary classification. Our framework enables domain experts or citizen scientists to iteratively label selected anomalies identified by the model during training, significantly improving detection performance through minimal additional labelling. Originally designed with astronomical datasets in mind, *AnomalyMatch* is highly generalizable to other domains with similar data characteristics. Moreover, our implementation prioritizes scalability: *AnomalyMatch* can efficiently process and analyse hundreds of millions of images on just one graphics card as demonstrated in the accompanying article [10], making it particularly suitable for upcoming large-scale astronomical surveys and data repositories.

We validate *AnomalyMatch* using two datasets: *miniImageNet* (a natural-image benchmark) and *GalaxyMNIST* (an astronomy-specific galaxy morphology dataset). Our experiments quantify anomaly detection performance via area under the receiver operating characteristic (AUROC) and area under the precision recall curve (AUPRC) metrics under severe class imbalance as well as an anomaly detection efficiency metric. These benchmark results clearly demonstrate the efficacy of our semi-supervised and active-learning-based approach. Furthermore, *AnomalyMatch* complements existing methods effectively; while frameworks like *PyOD* [11] or *Astronomy* [7] primarily rely on classical methods (e.g., Isolation Forest), *AnomalyMatch* combines semi-supervised and active learning with training a neural network. Thus, our method excels in targeted anomaly discovery, empowering users to define and detect anomalies of specific scientific interest rather than general statistical outliers.

Our primary contributions are:

- A novel semi-supervised anomaly detection pipeline (*AnomalyMatch*) combining *FixMatch*, EfficientNet, and active learning in a heavily optimised framework, effectively leveraging unlabelled data and greatly reducing labelling requirements.
- A GUI-based active learning loop enabling human experts (or citizen scientists) to iteratively guide anomaly selection and improve model performance during training.
- Comprehensive benchmarking of *AnomalyMatch* on both natural and astronomical image datasets, demonstrating excellent performance in terms of AUROC/AUPRC and anomaly detection efficiency with extremely limited labelled samples (five to ten labelled anomalies).
- A highly efficient and scalable implementation capable of analysing 100 million images within days [10], seamlessly integrated into ESA’s Datalabs platform.
- A detailed discussion on implications for future large-scale anomaly detection applications, including potential expansions to new data modalities, advanced architectures (e.g., vision transformers), and explainable AI.

2 Related Work

2.1 Anomaly Detection Methods

Methods for anomaly detection, also known as outlier detection, are typically classified based on their dependence on labelled data into supervised, semi-supervised, and unsupervised learning paradigms [1].

Unsupervised methods identify anomalies based solely on deviations from the normal data distribution without labelled examples. Classical approaches include One-Class SVM [12], Isolation Forest [4], and Local Outlier Factor (LOF) [13], extensively available in libraries such as *PyOD* [11]. While effective on lower-dimensional or structured datasets, these methods often struggle with complex high-dimensional data like images, where feature extraction and similarity metrics are more challenging [14, 15].

Supervised methods, which require extensive labelled datasets containing anomalies, generally yield higher accuracy. However, fully labelled datasets are often impractical due to the difficulty and cost associated with obtaining labelled anomalies [3].

Semi-supervised methods, using a limited number of labelled examples and abundant unlabelled data, balance performance and practicality [16]. Deep learning-based semi-supervised anomaly detection approaches, such as Deep SAD [3], incorporate few labelled anomalies to guide learned representations. Similarly, Astronomy [7] integrates active learning and semi-supervised learning principles into an astronomy-focused anomaly detection framework.

While classical approaches remain effective in simpler domains, neural networks have proven particularly promising for anomaly detection in complex, high-dimensional image data due to their inherent ability to learn rich, hierarchical representations from raw input [17].

2.2 Advances in Semi-Supervised Learning

General-purpose semi-supervised learning methods have rapidly advanced in recent years. Early SSL algorithms, including Π -Model, Pseudo-Label, VAT, Mean Teacher, and UDA, effectively leveraged unlabelled data through consistency regularization and pseudo-labelling [18, 19, 20]. Among these, FixMatch [5] has notably simplified the approach by combining consistency regularization and confidence-based pseudo-labelling. Specifically, FixMatch generates pseudo-labels from weakly augmented unlabelled data and strongly augmented versions and then trains the model to predict consistently on both, thus effectively making use of unlabelled data. This technique achieves state-of-the-art results on common benchmarks (e.g., CIFAR-10, SVHN) with minimal labelled examples.

Variants of FixMatch have been successfully applied to specific domains, such as remote sensing imagery [16], semantic segmentation [21, 22], and graph classification [23]. These adaptations highlight FixMatch’s flexibility in handling various data modalities and structured prediction tasks. The success of FixMatch and related approaches across diverse settings motivates their adaptation to anomaly detection tasks characterized by severe label scarcity and class imbalance. In this work, we leverage FixMatch by formulating anomaly detection as a two-class classification problem—“anomaly vs. normal”—thus fully exploiting the potential of SSL techniques in anomaly discovery.

Overall, our approach synthesizes state-of-the-art semi-supervised learning with domain-tailored active learning and scalable software implementation, bridging a methodological gap in anomaly detection efficacy, especially relevant to data-intensive scientific applications in domains such as astronomy.

3 Methods

Our anomaly detection system, *AnomalyMatch*, consists of a semi-supervised binary classifier (nominal vs. anomaly), using the FixMatch algorithm, combined with an active-learning loop and an intuitive guided user interface (GUI). We detail each component below, highlighting key design decisions.

3.1 FixMatch for Anomaly Detection

We base our training methodology on FixMatch [5], initially proposed for multi-class semi-supervised learning. We adapt it specifically to anomaly detection, treating the problem as a binary classification: “nominal” (regular data) vs. “anomaly” (rare, interesting data) with heavy class imbalance. We use a small labelled set $\mathcal{D}_L = \{(x_i, y_i)\}$ and a large unlabelled set $\mathcal{D}_U = \{u_j\}$, typically with $|\mathcal{D}_U| \gg |\mathcal{D}_L|$ and severe imbalance in favour of nominal examples. A practical difference to applying FixMatch in our scenario is that additional labels for nominal data are easier to obtain, whereas anomaly labels are often extremely scarce or difficult to expand due to their rarity. To handle this severe imbalance, we include oversampling using a weighted random sampler with occurrence-based sampling probabilities of anomalies / nominal samples during training.

Let $f_\theta(x)$ denote the neural network model with parameters θ , outputting the probability $p(y = \text{anomaly} | x)$ for input x . In each training step, unlabelled images from \mathcal{D}_U undergo weak augmentation (simple flips, crops) to generate pseudo-labels if the model’s predicted probabilities exceed a high-confidence threshold τ (e.g., 0.95). A corresponding strongly augmented image (applying substantial random transformations) is then fed into the network, enforcing consistency by training the model to match its predictions to the pseudo-labels.

The overall loss comprises supervised binary cross-entropy loss (on labelled data) and unsupervised consistency loss (on confident pseudo-labelled data):

$$L = L_{\text{sup}} + \lambda \cdot L_{\text{unsup}}$$

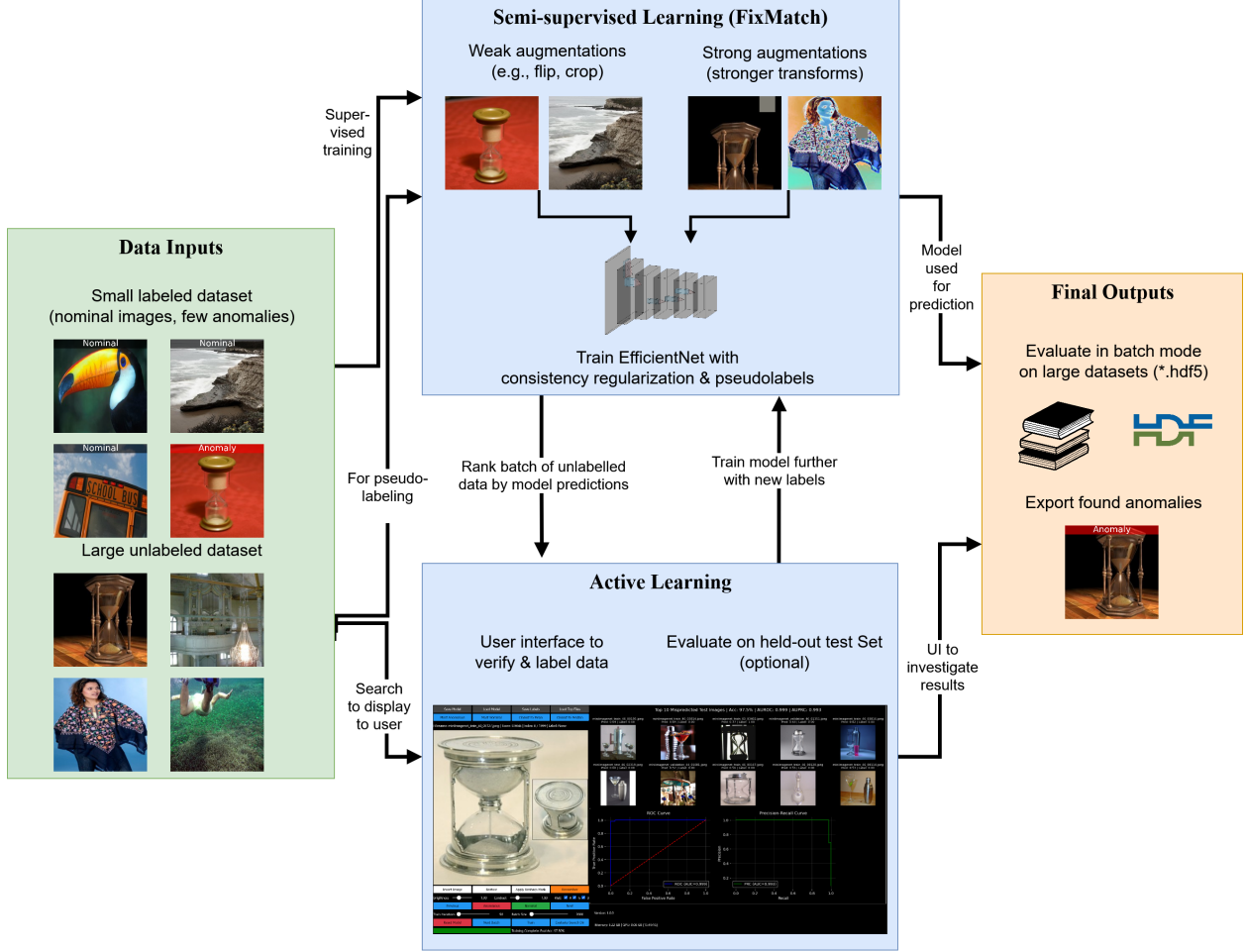


Figure 1: Overview of the AnomalyMatch workflow. A FixMatch-based semi-supervised learning loop trains an EfficientNet backbone using weak and strong augmentations. An active learning interface supports user verification and labelling of additional samples. The final model can be applied in batch mode to large datasets, with detected anomalies exported for further analysis.

We set use $\lambda = 1$ to emphasize unlabelled data contributions. Importantly, our experiments showed that training for fewer iterations (on the order of hundreds of iterations rather than tens of epochs until full convergence) is beneficial in the human-in-the-loop setup, as prolonged training sessions risk overfitting to the initial labels. This is explored in more detail in the Results Section.

3.2 EfficientNet Backbone

For computational efficiency and high accuracy, we chose EfficientNetLite0 [9], which achieves efficiency by systematically balancing depth, width, and resolution of the network through compound scaling, as our backbone convolutional neural network using input images resized to 224×224 . Smaller input sizes, such as 150×150 , were also successfully employed in our companion paper searching *Hubble Space Telescope* images [10]. The network is initialized using ImageNet pre-trained weights, fine-tuning all layers during FixMatch semi-supervised training. Weight decay (ℓ_2 regularization) is included to prevent overfitting.

3.3 Active Learning Loop and User Interface

Integrating human expertise is central to our pipeline. After initial training, the active learning loop identifies unlabelled images with the highest predicted anomaly scores, presenting them to the user through a dedicated interface (Figure 2).

Users verify and label anomalies, correcting false positives and confirming interesting candidates, thus efficiently refining the model.

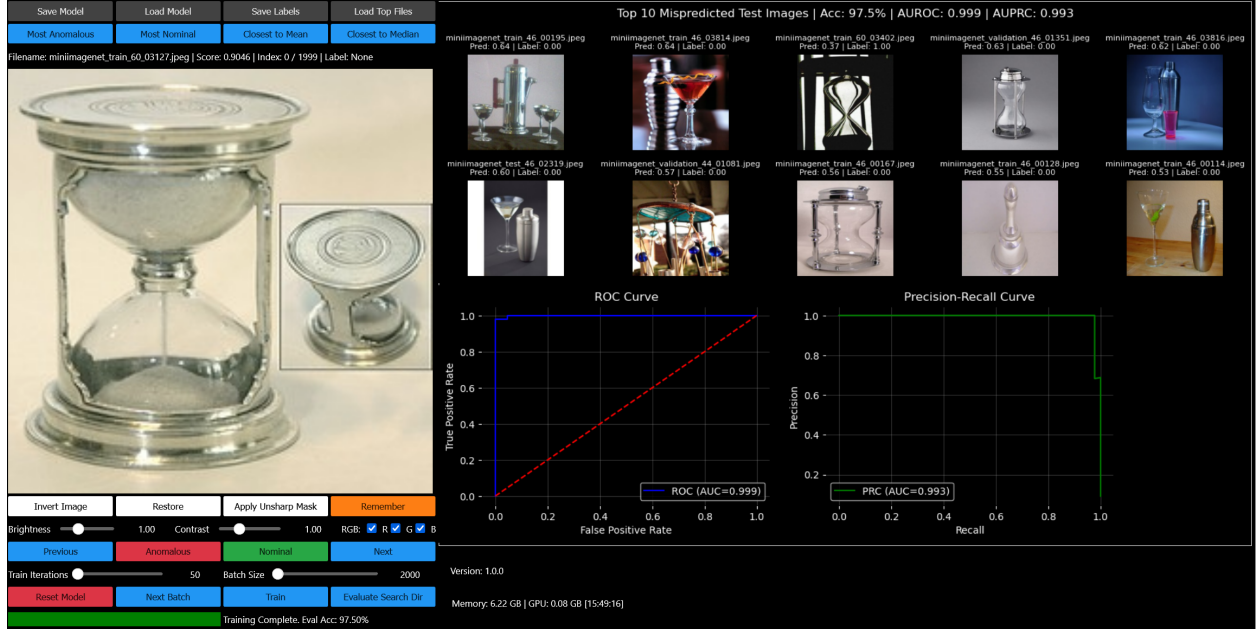


Figure 2: AnomalyMatch active learning interface built with *ipywidgets*. Users can inspect and label model-flagged candidates, adjust visual settings (e.g., brightness, contrast, RGB channels), and monitor performance via receiver operating characteristic and precision-recall curves. Model and label states can be saved and reloaded across sessions.

The GUI provides various practical features:

- **Image Processing Tools:** Adjustments for brightness, contrast, unsharp masking, and channel-specific filters (RGB) to support precise labelling.
- **Performance Feedback:** Immediate feedback through AUROC and AUPRC metrics if a held-out test set was defined initially.
- **Interactive Data Management:** Users can load batches of unlabelled data, save session labels and models, and iteratively continue cycles of labelling and retraining.

This user-friendly interface leverages *ipywidgets*, facilitating interactive exploration within Jupyter notebooks. A prebuilt setup integrated within the European Space Agency’s (ESA) Datalabs platform further provides seamless access to large-scale astronomical datasets, such as the recent Euclid Q1 data release [24], enabling immediate practical use in scientific analyses.

3.4 Data Augmentations

Robust data augmentation is essential to effective semi-supervised learning. We started from augmentation strategies validated by MSMATCH [16] and DistMSMATCH [25] for the two-tiered augmentation approach:

- **Weak Augmentations:** Minor transformations (horizontal flips, slight random crops) that preserve image content integrity, essential for accurate pseudo-label generation.
- **Strong Augmentations:** Applying RandAugment [26], we perform aggressive transformations including rotations, colour distortions (brightness, contrast, solarization), sharpness variations, shearing, translations, and posterization. These diverse distortions encourage model robustness and invariance to image variability.

3.5 Implementation and Scalability

Our pipeline is built to ensure scalability, robustness, and reproducibility. Initially derived and extensively refactored from an existing PyTorch implementation of FixMatch¹, our architecture has been optimized for large-scale datasets, supporting efficient handling of datasets on terabyte scale (e.g. 100 million *Hubble* images) [10]. We handle data in HDF5 format to optimise performance during training and inference [27].

Practically important hyperparameters include the number of unlabelled images per training iteration (limited by GPU memory) and image input sizes, which directly influence training efficiency. Supported input formats include single-channel and RGB imagery (PNG, TIFF, JPEG).

Continuous integration and continuous deployment workflows incorporating over 70 unit tests ensure code robustness, reliability, and maintainability. This is essential given the complex interaction of semi-supervised and active learning components. Pending ESA licensing processes, the complete source code will be publicly available on GitHub², encouraging community collaboration and ongoing development.

4 Results

4.1 Datasets and Experimental Setup

We evaluate AnomalyMatch on two diverse datasets, one related to our primary application area in astronomy (GalaxyMNIST), and one standard benchmark commonly used in machine learning research (miniImageNet). MiniImageNet was specifically chosen as it is computationally more tractable than the full ImageNet dataset, making it well-suited for our experimentation.

GalaxyMNIST [28] comprises annotated greyscale galaxy images derived from the Galaxy Zoo citizen science project [8]. Images originally have a resolution of 64×64 pixels, which we upsampled to 224×224 pixels for consistency across experiments. The dataset contains four morphological classes annotated by volunteers: Smooth Round, Smooth Cigar-shaped, Edge-on Disk, and Unbarred Spiral. For evaluation, we treated each morphological type sequentially as anomalies, using the other three classes as nominal samples.

miniImageNet [29] is a widely used benchmark in few-shot learning. It consists of colour images grouped into 100 classes and is taken from the larger ImageNet dataset. Each image was resized from its original resolution to 224×224 pixels. We deliberately selected five distinct object classes as anomalies to evaluate our model’s performance across diverse visual features: piano, hourglass, guitar, printer, and orange.

Figure 3 shows representative examples from both datasets.

For GalaxyMNIST, we started experiments with a small labelled set of 40 images (10 anomalies, 30 nominal). For miniImageNet, initial labelled data included 500 images (five anomalies, 495 nominal). In both cases, each training step utilised an additional randomly sampled pool of 10,000 unlabelled images.

To simulate active learning, we performed three consecutive training cycles of 100 iterations each. After each cycle, the 10 highest-scoring anomalies and 10 highest-scoring false positives (nominal images with high anomaly classification scores by the model) were labelled and incorporated into the training set for the next cycle. The models are finally evaluated on all unlabelled images.

The FixMatch algorithm [5] formed the basis of our semi-supervised training procedure. Key hyperparameters included an exponential moving average (EMA) momentum of 0.99, confidence threshold (τ) of 0.95, temperature of 0.5, unsupervised-to-supervised loss ratio of 1.0, a batch size of 16, learning rate of 0.0075 (with SGD optimizer, momentum 0.9), and weight decay of 7.5×10^{-4} . We followed empirical results from [16, 25] in the selection of parameters.

Throughout the experiments, we employed three key metrics: Area Under the Receiver Operating Characteristic (AUROC), Area Under the Precision-Recall Curve (AUPRC), and Anomaly Detection Efficiency. AUROC and AUPRC provide complementary views of classification performance, especially important under severe class imbalance. Anomaly Detection Efficiency quantifies the fraction of anomalies correctly identified within a specified percentage of top-scoring samples, directly reflecting practical usefulness in scenarios involving human-in-the-loop validation and limited labelling resources.

¹<https://github.com/LeeDoYup/FixMatch-pytorch> — PyTorch code for FixMatch (Accessed 2025-03-28)

²<https://github.com/esa/AnomalyMatch>

GalaxyMNIST

Anomaly Classes in Red

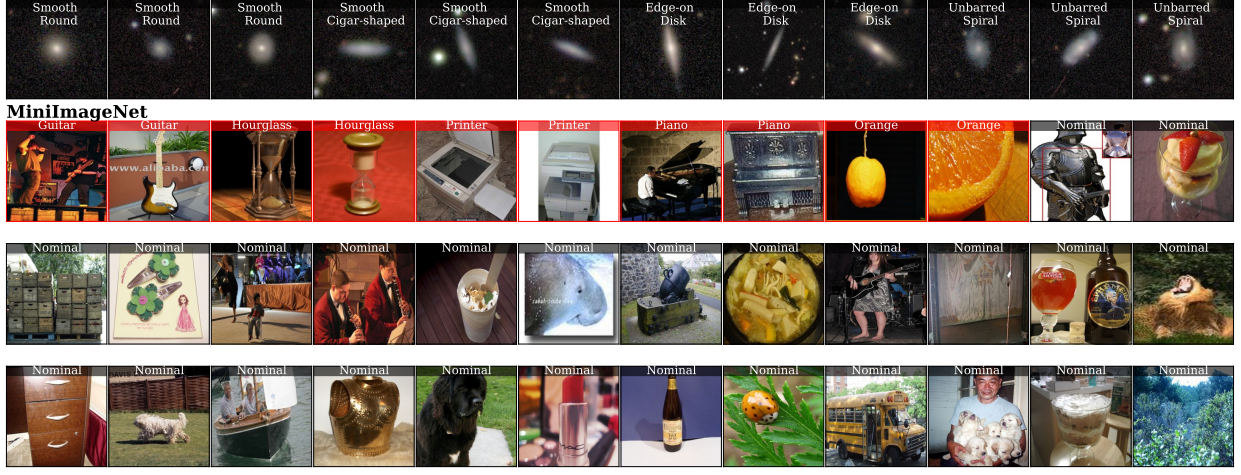


Figure 3: Sample images from GalaxyMNIST (top) and MiniImageNet (bottom). Red borders indicate anomaly classes used during evaluation, while nominal samples are shown with white borders. For GalaxyMNIST all classes were tested as anomaly class in a dedicated run.

$$\text{AUROC} = \int_0^1 \text{TPR}(t) d\text{FPR}(t)$$

$$\text{AUPRC} = \int_0^1 \text{Precision}(r) d\text{Recall}(r)$$

$$\text{Efficiency at } p\% = \frac{\text{Number of anomalies in top } p\% \text{ of scores}}{\text{Total number of anomalies}} \times 100\%$$

where:

- $\text{TPR}(t) = \frac{\text{TP}(t)}{\text{TP}(t) + \text{FN}(t)}$ (true positive rate, also called recall)
- $\text{FPR}(t) = \frac{\text{FP}(t)}{\text{FP}(t) + \text{TN}(t)}$ (false positive rate)
- $\text{Precision}(t) = \frac{\text{TP}(t)}{\text{TP}(t) + \text{FP}(t)}$
- $\text{Recall}(t) = \text{TPR}(t)$
- $\text{FPR}^{-1}(x)$ is the threshold value that gives an FPR of x
- $\text{Recall}^{-1}(r)$ is the threshold value that gives a Recall of r

and $t \in [0, 1]$ represents the classification threshold, and TP, FP, TN, FN denote counts of true positives, false positives, true negatives, and false negatives at threshold t .

4.2 miniImageNet Results

We summarize our experimental results on the miniImageNet dataset, focusing initially on the class *hourglass* as a representative example. Results for the other evaluated anomaly classes (printer, piano, guitar, and orange) are presented in Table 1.

Performance Metrics and Efficiency We evaluate anomaly detection performance using the AUROC, AUPRC, and the anomaly detection efficiency metrics. Anomaly detection efficiency, a practical measure for real-world applications, quantifies the fraction of anomalies identified within the highest-scoring fraction of the dataset. Given the severe class

Table 1: Evaluation on unlabelled data for miniImageNet with different classes used as anomaly after three iterations with active learning. At 100% precision no more anomalies could have been found in the top-scoring 0.1% or 1% of the dataset, respectively. Training started from five labelled anomalies, adding ten after each iteration.

Anomaly Class	AUROC	AUPRC	Anomalies in top-scoring 0.1% [%]	Precision in top-scoring 0.1% [%]	Anomalies in top-scoring 1% [%]	Precision in top-scoring 1% [%]
Guitar	0.95	0.76	10.24	100.00	72.32	70.19
Hourglass	0.96	0.80	10.24	100.00	74.72	72.52
Printer	0.98	0.86	10.24	100.00	81.44	79.04
Piano	0.95	0.75	10.24	100.00	71.36	69.25
Orange	0.92	0.65	10.24	100.00	64.16	62.27
Mean	0.95 ± 0.02	0.76 ± 0.08	10.24 ± 0.00	100.00 ± 0.00	72.80 ± 6.23	70.65 ± 6.05

imbalance (approximately 1% anomalies), high performance under this metric is critical to minimise manual inspection by domain experts.

Figure 4 shows representative receiver operation characteristic and Precision-Recall curves for the *hourglass* anomaly class after the final active learning cycle. Our approach achieved an AUROC of 0.96 and AUPRC of 0.80, indicating strong separation between nominal and anomalous samples.

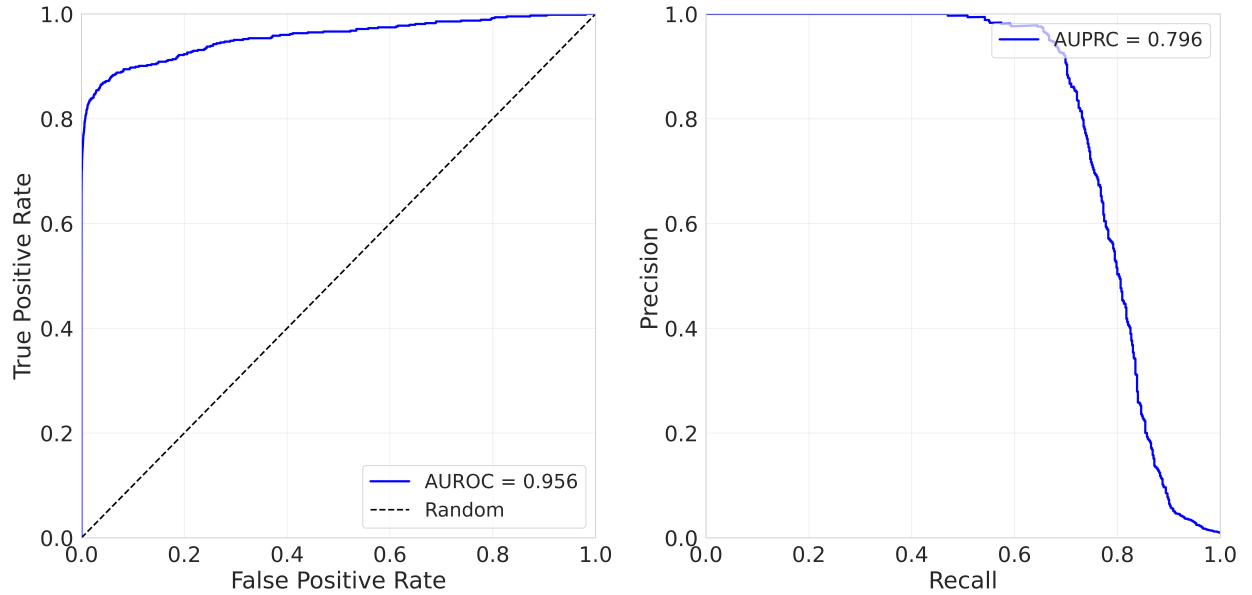
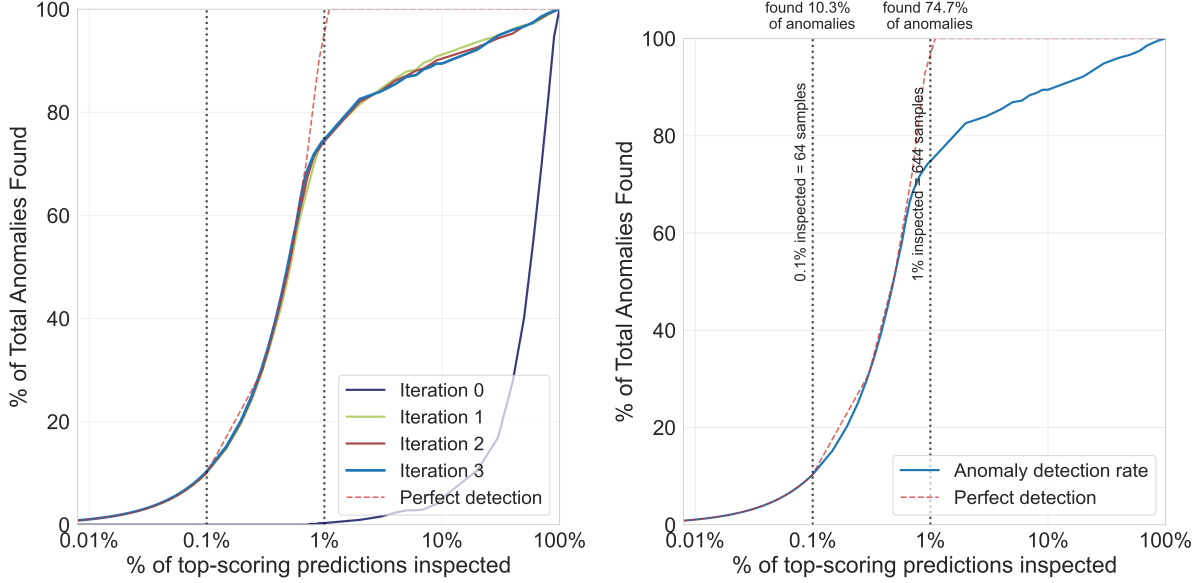


Figure 4: Receiver operation characteristic (left) and Precision-Recall (right) curves after three active learning cycles for the miniImageNet ‘hourglass’ anomaly class starting from five labelled anomalies, adding ten after each iteration. The model achieves an AUROC of 0.96 and an AUPRC of 0.80, highlighting robust anomaly detection capability under severe class imbalance.

Figure 5 shows the anomaly detection efficiency curve after three iterations for the hourglass anomaly class. Remarkably, the method identifies 74.7% of anomalies within the top 1% highest-scoring images, demonstrating very high capability to retrieve relevant anomalies for the user. The top-scoring 0.1% data samples are all correctly identified anomalies. Successive active learning only marginally increase performance. A likely reason seems that learning gains from the initial sampling data, which remain the majority of labelled data throughout, can already be achieved within the first iteration.

Table 1 summarizes performance metrics across all tested anomaly classes. The model consistently achieves high AUROC and AUPRC values, identifying approximately three-quarters of anomalies in the top 1% scoring images, and attaining precision between 65% and 81%. Average precisions for the top-scoring 0.1% of the data were 99.7%. This indicates strong practical utility for human reviewers who would want to quickly identify additional anomalies.



(a) Efficiency progression across iterations: efficiency improves quickly, with strong performance already after the first iteration. The red dashed line represents perfect detection performance. 10.3% already recovered in the top 0.1%. (b) Final performance after three iterations: 74.7% of all anomalies are found within the top 1% of the ranked predictions, with

Figure 5: Anomaly detection efficiency curves for the *Hourglass* class in miniImageNet. Each point on the x-axis represents a percentage of the ranked predictions inspected, sorted by descending anomaly score (i.e., the most anomalous images are checked first). The y-axis shows the percentage of true anomalies recovered within the inspected data subset. Active learning started with five labelled anomalies and adds ten samples after each iteration.

In summary, these results demonstrate the effectiveness of our approach, highlighting its practical value by consistently ranking most anomalies highly and significantly reducing the labelling workload required from human experts for enabling such a result by starting from only five labelled samples.

4.3 GalaxyMNIST Results

For GalaxyMNIST, we illustrate our results using the *Unbarred Spiral* class as representative anomalies from the dataset. Notably, in this case the fraction of anomalies in the dataset (25%) is much higher compared to miniImageNet (1%).

Performance Metrics and Efficiency Receiver operation characteristic and Precision-Recall curves (Figure 6) confirm the robustness of the model. Despite GalaxyMNIST’s classes being visually similar and challenging to distinguish even for human observers, the model achieves strong discrimination performance (AUROC: 0.889, AUPRC: 0.774), significantly above random chance.

Figure 7 shows how anomaly detection efficiency evolves across iterations. A clear improvement of the model is visible after each active learning step, indicating significantly enhanced anomaly ranking capabilities.

The final anomaly detection efficiency curve in Figure 7 demonstrates strong final performance, particularly at lower inspection percentages. Remarkably, within the top 0.1% highest-scoring samples, 100% precision was achieved, thus successfully identifying anomalies immediately within a very small subset of the data. Successive active learning continue to increase performance in contrast to the experiments on MiniImageNet. One potential reason may lie in the overall greater number of anomalous samples in the dataset, leading to a potentially higher heterogeneity of anomalies.

Table 2 summarises results across all anomaly classes of GalaxyMNIST.

Overall, anomaly detection performance on GalaxyMNIST varied between classes, reflecting visual and morphological similarities inherent in the dataset. Notably, three out of four classes achieved perfect anomaly detection precision within the top 0.1% of highest-scoring samples, demonstrating excellent efficiency in scenarios where quick anomaly identification from large data pools is required. Conversely, classes like *Smooth Cigar-shaped* and *Edge-on Disk* led to

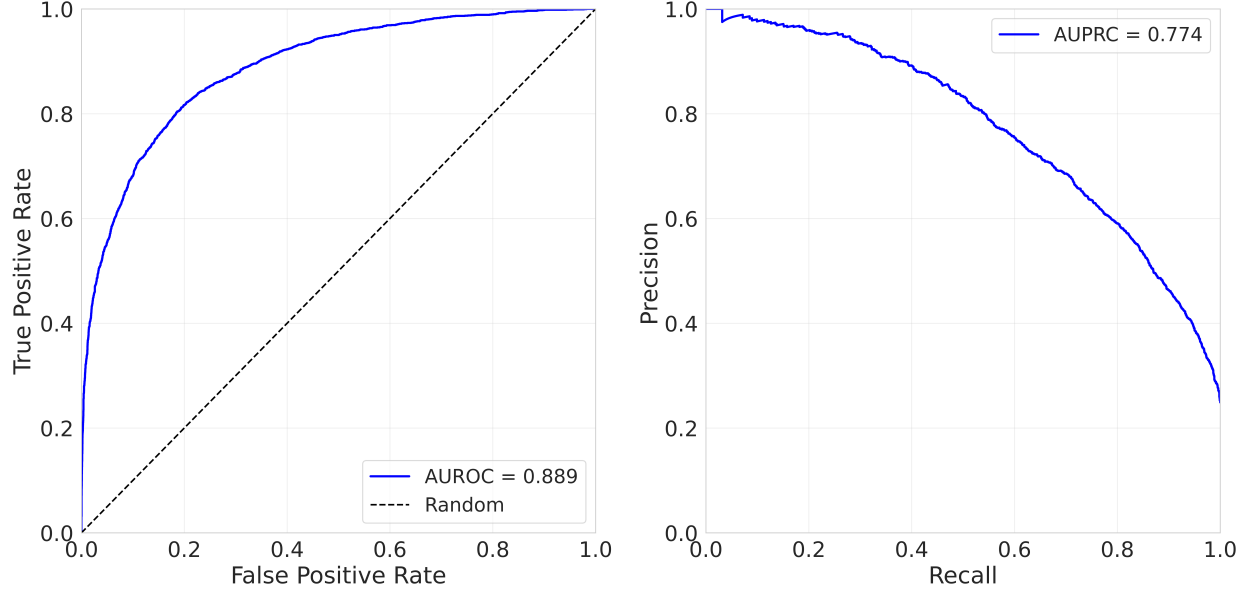
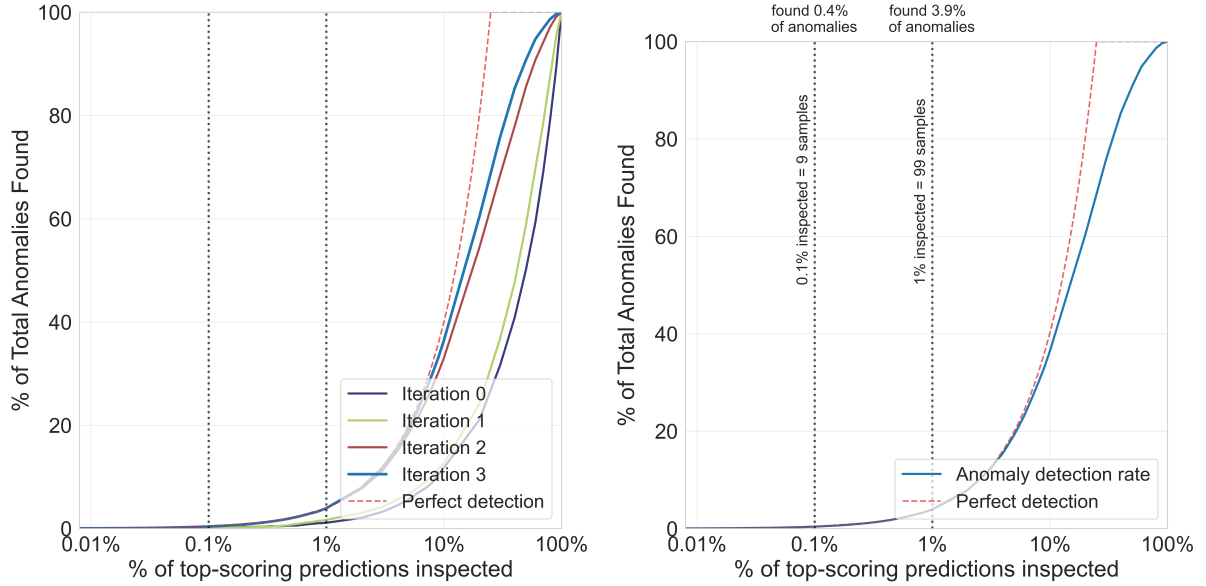


Figure 6: Receiver operation characteristic (left) and Precision-Recall (right) curves for the *Unbarred Spiral* anomaly class from GalaxyMNIST. High AUROC and AUPRC indicate effective anomaly identification despite the inherent morphological similarities across galaxy classes. Training started from ten labelled anomalies, adding ten after each iteration.



(a) Active learning efficiency across iterations: progressive improvements are visible over three iterations, with more anomalies recovered early in the ranked predictions. (b) Final performance after three iterations: within the top 1% of the ranked predictions only anomalies are found

Figure 7: Anomaly detection efficiency curves for the *Unbarred Spiral* class in GalaxyMNIST. The x-axis shows the percentage of the data inspected, sorted by descending predicted anomaly score, while the y-axis reflects the cumulative percentage of true anomalies recovered. The model is trained using ten labelled anomalies initially, with ten more added after each active learning cycle.

Table 2: Evaluation on unlabelled data for GalaxyMNIST with different classes used as anomaly after three iterations with active learning. At 100% precision no more anomalies could have been found in the top-scoring 0.1% or 1% of the dataset, respectively. Training started from ten labelled anomalies, adding ten after each iteration.

Anomaly Class	AUROC	AUPRC	Anomalies in top-scoring 0.1% [%]	Precision in top-scoring 0.1% [%]	Anomalies in top-scoring 1% [%]	Precision in top-scoring 1% [%]
Smooth Round	0.97	0.91	0.36	100.00	3.97	98.99
Smooth Cigar-shaped	0.75	0.51	0.28	77.78	3.36	83.84
Edge-on Disk	0.85	0.66	0.36	100.00	3.72	92.93
Unbarred Spiral	0.89	0.77	0.36	100.00	3.93	97.98
Mean	0.86 ± 0.09	0.71 ± 0.17	0.34 ± 0.04	94.44 ± 11.11	3.75 ± 0.28	93.44 ± 6.92

Table 3: Effect of size of initial labelled dataset on anomaly detection performance in MiniImageNet. Each configuration starts with a different number of labelled samples and adds different number of labels per iteration. Despite large differences in initial label counts, performance remains robust across metrics, with perfect precision at the top 0.1% most anomalous samples for all scenarios. Beyond 500 (+20) labels no performance gains are observed.

Labels	AUROC	AUPRC	Anomalies in top-scoring 0.1% [%]	Precision in top-scoring 0.1% [%]	Anomalies in top-scoring 1% [%]	Precision in top-scoring 1% [%]
100 (1 / 99) + 10 per iteration	0.93	0.65	10.02	100.00	61.66	60.80
500 (5 / 495) + 20 per iteration	0.96	0.79	10.24	100.00	75.20	72.98
1000 (10 / 990) + 40 per iteration	0.95	0.78	10.50	100.00	75.00	70.42
Mean	0.95 ± 0.02	0.74 ± 0.08	10.25 ± 0.24	100.00 ± 0.00	70.62 ± 7.76	68.07 ± 6.42

lower AUROC and AUPRC values, highlighting the inherent difficulty and potential ambiguity in visually separating these morphologies.

4.4 Ablation Studies

To evaluate the robustness and practical sensitivity of our approach to key training parameters, we conducted targeted ablation studies on the miniImageNet dataset, specifically focusing on the class *guitar* as anomalies. This class was picked as we achieved median performance on it.

4.4.1 Number of Initial Labels

We investigated the impact of varying the number of initial labels while maintaining the proportion of anomalies within these labels. Three scenarios were tested: 100 initial labels (one anomaly, 99 nominal), 500 initial labels (five anomalies, 495 nominal), and 1000 initial labels (10 anomalies, 990 nominal). After each active learning cycle, we correspondingly increased the number of actively labelled samples per iteration proportionally to the initial sample size: 10 additional labels per iteration for the smallest set, 20 labels for the intermediate set, and 40 labels for the largest set.

Detailed results for these ablations are summarised in Table 3.

Interestingly, we observed limited differences in performance metrics across all tested initial labelling conditions. AUROC and AUPRC values varied by less than 0.03, and anomaly detection efficiency remained consistently high. Notably, all experiments achieved perfect precision at the stringent threshold of inspecting just the top 0.1% scoring data points, further underscoring the robustness and consistency of our active learning pipeline. This indicates our approach effectively utilises available labels and does not significantly benefit from substantially larger initial label sets, highlighting its practical efficacy even with minimal labelled data.

Table 4: Impact of FixMatch training duration per active learning step. Performance peaks at shorter training cycles (50–100 iterations), with diminishing returns and mild overfitting at longer durations. This supports our design choice of brief, iterative updates with rapid model adaptation.

Iterations	AUROC	AUPRC	Anomalies in top-scoring 0.1% [%]	Precision in top-scoring 0.1% [%]	Anomalies in top-scoring 1% [%]	Precision in top-scoring 1% [%]
50	0.97	0.77	10.24	100.00	71.52	69.41
100	0.97	0.79	10.24	100.00	74.72	72.52
250	0.95	0.78	10.24	100.00	74.08	71.89
500	0.94	0.77	10.24	100.00	73.44	71.27
Mean	0.96 ± 0.02	0.78 ± 0.01	10.24 ± 0.00	100.00 ± 0.00	73.44 ± 1.38	71.27 ± 1.34

Table 5: Comparison of anomaly detection performance with and without active learning. Active learning at same starting labels yields higher AUPRC and precision within the top 1% most anomalous predictions. Using all actively gathered labels for semi-supervised training yields the highest performance, suggesting benefits from iterative human-in-the-loop feedback and re-use of confirmed anomalies.

Active Learning	AUROC	AUPRC	Anomalies in top-scoring 0.1% [%]	Precision in top-scoring 0.1% [%]	Anomalies in top-scoring 1% [%]	Precision in top-scoring 1% [%]
Active Learning	0.96	0.79	10.24	100.00	74.56	72.36
No Active Learning (same starting samples)	0.96	0.70	9.77	98.44	65.89	65.89
No Active Learning (same total samples)	0.99	0.85	10.41	100.00	78.70	75.16
Mean	0.97 ± 0.02	0.78 ± 0.08	10.14 ± 0.33	99.48 ± 0.90	73.05 ± 6.54	71.14 ± 4.75

4.4.2 Training Iterations

To assess how training duration per cycle affects anomaly detection, we varied the number of FixMatch training iterations per cycle across four settings: 50, 100, 250, and 500. Results are presented in Table 4.

We observe that performance peaks at around 100 training iterations per cycle. Using more iterations results in slightly worse AUROC and AUPRC, which we attribute to overfitting on the initially provided labelled data. As the active learning loop dynamically updates the training set, excessively long training phases may entrench early biases. This supports our design choice of short training cycles, encouraging the model to adapt quickly to newly labelled examples.

4.4.3 Impact of Active Learning

We specifically investigated the impact of incorporating active learning by comparing our standard iterative labelling approach against two pure semi-supervised scenarios without additional human-in-the-loop labels, one with the same amount of initial labels and, respectively, same final amount (i.e. total number including those added during active learning). Figure 8 illustrates anomaly detection efficiency for those scenarios.

While passive training (no additional active learning) yielded similar AUROC and AUPRC metrics, active learning exhibited significantly improved practical efficiency in regard to anomaly detection efficiency. Crucially, in the most relevant operational range (inspecting the top 0.1%–1% of scored samples), active learning consistently ranked more anomalies higher for the same starting samples. For instance, active learning allowed users to detect 75% of anomalies within the top 1% of the ranked dataset, while the passive model lagged behind in top-scoring predictions’ precision (particularly visible in the 0.1% inspection range).

This highlights a critical trade-off: despite marginally lower overall metric scores, the actively updated model significantly reduces human inspection efforts by focusing the user’s attention effectively, thus strongly supporting the use of active learning in real-world applications. However, retraining with all found anomalies still yields the best performance, likely due to a more balanced representation of anomaly samples during training.

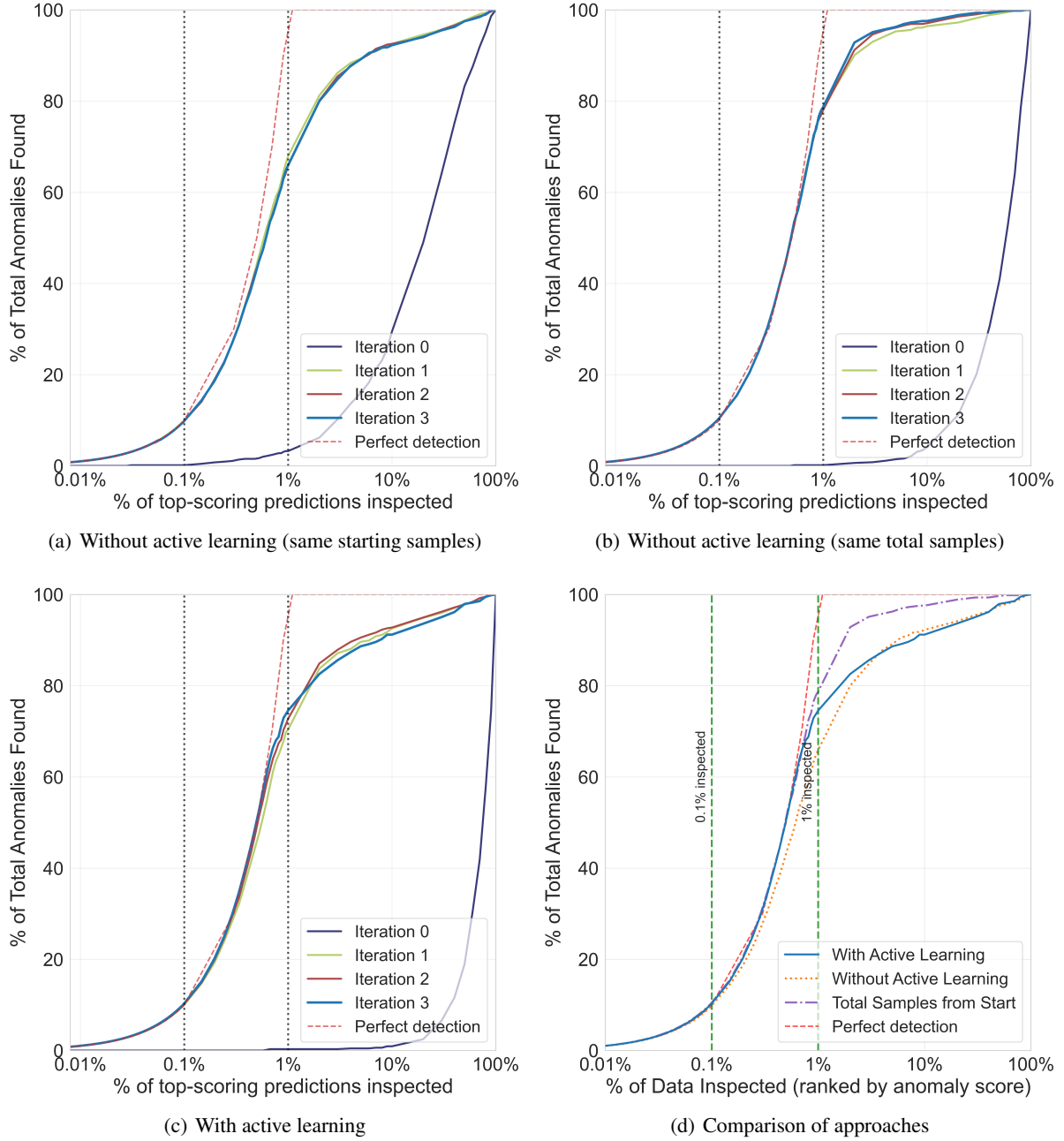


Figure 8: Anomaly detection efficiency comparison with and without active learning. The actively learned model achieves notably better efficiency within the crucial 0.1–1% data inspection range for the same starting labels (compare (a) and (c)), indicating a meaningful advantage in human-in-the-loop anomaly searches. However, training with the full set of labels (as would be identified during active learning) from scratch leads to the best performance (b), highlighting the potential of re-using found anomalies in new semi-supervised runs. The direct comparison in (d) further illustrates the relative performance across all approaches, demonstrating how active learning bridges the gap between limited-label and full-label scenarios.

4.5 Discussion

Our results highlight the practical efficiency and robustness of the AnomalyMatch framework, demonstrating significant potential to substantially reduce the manual review burden for anomaly identification tasks. The method efficiently leverages both computational resources and human labelling effort, achieving strong performance even with very limited labelled data. Crucially, our experiments reveal diminishing returns from significantly increasing the number of initial labels. This effect is consistent with earlier findings in semi-supervised learning theory and empirical studies that suggest performance gains saturate quickly beyond a modest label count [30]. This outcome underscores the method's effective utilisation of limited supervision, suggesting that label sparsity — a common real-world constraint — is not a major limitation in practice.

The integration of active learning notably enhances anomaly detection efficiency, particularly in the critical inspection range (top 0.1%–1% of ranked data). While active learning's impact on global performance metrics such as AUROC and AUPRC might appear moderate, its practical value in real-world scenarios cannot be overstated, as domain experts typically inspect only a small fraction of data. Thus, actively guided iterative labelling can substantially increase the productivity of domain experts, aligning well with real-world needs.

A key finding of our study is the pronounced risk of overfitting when extending training beyond the optimal number of iterations per active learning cycle. Notably, our experiments suggest the ideal balance is around 100 iterations per active learning cycle; longer cycles appear to reduce overall anomaly detection efficiency, highlighting the need for careful tuning and early stopping strategies. Such overfitting risk in SSL has been previously observed, especially in low-label regimes without strong regularisation [31]. Given that original FixMatch and its derivatives such as MSMatch typically employ extensive training iterations, our adaptation of shorter, frequent retraining cycles emerges as a beneficial modification tailored to active learning scenarios with heavily imbalanced classes and a simplified binary classification task.

Additionally, while we have demonstrated effectiveness across datasets with drastically different class imbalance characteristics — extremely skewed (miniImageNet) and moderately balanced (GalaxyMNIST) — further research is necessary to investigate the lower bounds of label numbers needed for robust anomaly detection performance. Preliminary findings from an accompanying paper focused on the *Hubble Space Telescope* dataset [10] suggest that AnomalyMatch might remain effective with even fewer initial labels, further reducing labelling costs. There, we also utilised a hybrid approach: initially using active learning to identify a sufficient number of anomalies, then transitioning to a fully semi-supervised regime for optimal performance.

4.6 Limitations

Despite strong results, our study acknowledges several important limitations that warrant further exploration:

Idealised Active Learning Assumptions: Our experiments assumed an idealised active learning environment where human annotations are consistently accurate. In practical deployments, labelling errors and inconsistencies are likely, particularly in ambiguous cases. Additionally, our experiments assumed balanced incremental labelling (equal numbers of anomalies and nominal cases per active learning cycle), which may differ significantly in real-world usage where nominal labels are generally easier and cheaper to obtain than anomalies.

Pretraining Bias: Performance on the miniImageNet dataset likely benefits from the EfficientNet backbone's ImageNet pretraining. Such pretrained representations inherently capture generic features beneficial for image classification, possibly inflating performance metrics. Future studies should assess performance sensitivity when employing randomly initialised neural networks or representations pretrained on domain-specific data.

Limited Exploration of Class Imbalance Scenarios: While we investigated datasets at two extremes of class imbalance (1% vs. 25% anomalies), real-world anomaly scenarios may present even more extreme imbalance, significantly affecting performance. Additional research is needed to characterise model behaviour across a broader spectrum of imbalance ratios.

Anomaly Homogeneity Assumption: We simplified the anomaly detection task by treating all anomalies as belonging to a single implicit category distinct from nominal instances. This assumption might limit applicability in scenarios with highly heterogeneous anomalies, each requiring distinct learned representations. Incorporating methods explicitly capable of handling diverse anomaly categories could enhance generalisation.

Impact of Labelling Errors: Our study does not examine the robustness of AnomalyMatch to labelling inaccuracies, an important consideration given the potential for human annotation errors during active learning. Exploring training strategies that explicitly handle or mitigate labelling noise is necessary for real-world robustness.

Addressing these limitations in future work will further strengthen the practical applicability of our approach, enabling its robust deployment in diverse, realistic scientific and industrial contexts.

5 Conclusion and Outlook

In this study, we introduced AnomalyMatch, a robust semi-supervised active learning framework tailored for efficiently identifying anomalies in large-scale image datasets. Our pipeline, combining FixMatch-based semi-supervised learning, EfficientNet as a computational backbone, and an interactive graphical user interface, demonstrated excellent performance across diverse datasets (GalaxyMNIST and miniImageNet), highlighting its capability to effectively operate under severe class imbalance and label scarcity—conditions frequently encountered in astronomy. By significantly reducing the manual review burden, AnomalyMatch offers substantial potential to streamline anomaly discovery processes, effectively harnessing minimal human input and maximising the efficiency of scarce domain-expert resources.

Looking ahead, several promising opportunities exist to further refine and extend the capabilities of AnomalyMatch. Incorporating explainable AI methods, such as attention maps, SHAP [32] values, or feature attribution techniques, could provide crucial interpretability and insight into model decision-making, increasing trust and facilitating model validation by domain experts. Additionally, extending the model to handle multimodal data—such as integrating image information with complementary spectral or time-series data—would allow richer contextual analysis, potentially enhancing anomaly detection accuracy in complex scientific scenarios. Further improvements could come from developing adaptive training strategies that dynamically calibrate training steps and parameters in response to real-time performance metrics, thus mitigating overfitting risks identified in our current approach. Finally, establishing curated, dedicated benchmark datasets with expert-validated labels, particularly in astronomy, would significantly support methodological advancements, comparison, and standardisation within the anomaly detection research community. Pursuing these enhancements will solidify AnomalyMatch as a versatile and impactful framework, beneficial not only to astronomy but broadly to scientific domains confronted with similar data challenges.

Acknowledgments

This work made use of AI tools for code generation and writing support. The authors would like to acknowledge valuable feedback received from Pedro Mas Buitrago, Laslo Erik Ruhberg and Maria Teresa Nardone.

References

- [1] Varun Chandola, Arindam Banerjee, and Vipin Kumar. Anomaly detection: A survey. *ACM computing surveys (CSUR)*, 41(3):1–58, 2009.
- [2] Marco AF Pimentel, David A Clifton, Lei Clifton, and Lionel Tarassenko. A review of novelty detection. *Signal processing*, 99:215–249, 2014.
- [3] Lukas Ruff, Robert A. Vandermeulen, Nico Görnitz, Alexander Binder, Emmanuel Müller, Klaus-Robert Müller, and Marius Kloft. Deep semi-supervised anomaly detection. In *8th International Conference on Learning Representations (ICLR)*, 2020. URL <https://openreview.net/forum?id=HkgHOTEYwH>.
- [4] Fei Tony Liu, Kai Ming Ting, and Zhi-Hua Zhou. Isolation forest. In *2008 eighth ieee international conference on data mining*, pages 413–422. IEEE, 2008.
- [5] Kihyuk Sohn, David Berthelot, Nicholas Carlini, Zizhao Zhang, Han Zhang, Colin A Raffel, Ekin Dogus Cubuk, Alexey Kurakin, and Chun-Liang Li. Fixmatch: Simplifying semi-supervised learning with consistency and confidence. *Advances in neural information processing systems*, 33:596–608, 2020.
- [6] Burr Settles. Active learning literature survey. 2009.
- [7] Michelle Lochner and Bruce A Bassett. Astronomaly: Personalised active anomaly detection in astronomical data. *Astronomy and Computing*, 36:100481, 2021.
- [8] Chris J Lintott, Kevin Schawinski, Anže Slosar, Kate Land, Steven Bamford, Daniel Thomas, M Jordan Raddick, Robert C Nichol, Alex Szalay, Dan Andreescu, et al. Galaxy zoo: morphologies derived from visual inspection of galaxies from the sloan digital sky survey. *Monthly Notices of the Royal Astronomical Society*, 389(3):1179–1189, 2008.

- [9] Mingxing Tan and Quoc Le. Efficientnet: Rethinking model scaling for convolutional neural networks. In *International conference on machine learning*, pages 6105–6114. PMLR, 2019.
- [10] David O’Ryan and Pablo Gomez. Applying anomaly detection to the hubble legacy archive. 2025. arXiv preprint arXiv:PLACEHOLDER.
- [11] Yue Zhao, Zain Nasrullah, and Zheng Li. Pyod: A python toolbox for scalable outlier detection. *Journal of machine learning research*, 20(96):1–7, 2019.
- [12] Bernhard Schölkopf, John C Platt, John Shawe-Taylor, Alex J Smola, and Robert C Williamson. Estimating the support of a high-dimensional distribution. *Neural computation*, 13(7):1443–1471, 2001.
- [13] Markus M Breunig, Hans-Peter Kriegel, Raymond T Ng, and Jörg Sander. Lof: identifying density-based local outliers. In *Proceedings of the 2000 ACM SIGMOD international conference on Management of data*, pages 93–104, 2000.
- [14] Markus Goldstein and Seiichi Uchida. A comparative evaluation of unsupervised anomaly detection algorithms for multivariate data. *PLOS ONE*, 11(4):e0152173, 2016. doi: 10.1371/journal.pone.0152173.
- [15] Arthur Zimek, Erich Schubert, and Hans-Peter Kriegel. A survey on unsupervised outlier detection in high-dimensional numerical data. *Statistical Analysis and Data Mining: The ASA Data Science Journal*, 5(5):363–387, 2012. doi: 10.1002/sam.11161.
- [16] Pablo Gómez and Gabriele Meoni. MSMatch: Semi-supervised multispectral scene classification with few labels. *IEEE Journal of Selected Topics in Applied Earth Observations and Remote Sensing*, 14:11643–11654, 2021. doi: 10.1109/JSTARS.2021.3126082.
- [17] Songqiao Han, Xiyang Hu, Hailiang Huang, Minqi Jiang, and Yue Zhao. Adbench: Anomaly detection benchmark. *Advances in neural information processing systems*, 35:32142–32159, 2022.
- [18] David Berthelot, Nicholas Carlini, Ian Goodfellow, Nicolas Papernot, Avital Oliver, and Colin A Raffel. Mixmatch: A holistic approach to semi-supervised learning. *Advances in neural information processing systems*, 32, 2019.
- [19] David Berthelot, Nicholas Carlini, Ekin D Cubuk, Alex Kurakin, Kihyuk Sohn, Han Zhang, and Colin Raffel. Remixmatch: Semi-supervised learning with distribution alignment and augmentation anchoring. *arXiv preprint arXiv:1911.09785*, 2019.
- [20] Qizhe Xie, Zihang Dai, Eduard Hovy, Thang Luong, and Quoc Le. Unsupervised data augmentation for consistency training. *Advances in neural information processing systems*, 33:6256–6268, 2020.
- [21] Miquel Martí i Rabadán, Alessandro Pieropan, Hossein Azizpour, and Atsuto Maki. Dense fixmatch: a simple semi-supervised learning method for pixel-wise prediction tasks. *arXiv preprint arXiv:2210.09919*, 2022.
- [22] Lihe Yang, Lei Qi, Litong Feng, Wayne Zhang, and Yinghuan Shi. Revisiting weak-to-strong consistency in semi-supervised semantic segmentation. *arXiv preprint arXiv:2208.09910*, 2022.
- [23] Saeid Jalali, Jianhao Wu, Ahmad Dargahi Nobari, and Baris Fidan. Graphixmatch: Semi-supervised graph classification with fixmatch. *Neurocomputing*, 2024. doi: 10.1016/j.neucom.2024.127186.
- [24] H Aussel, I Tereno, M Schirmer, G Alguero, B Altieri, E Balbinot, T de Boer, P Casenove, P Corcho-Caballero, H Furusawa, et al. Euclid quick data release (q1)-data release overview. *arXiv preprint arXiv:2503.15302*, 2025.
- [25] Johan Östman, Pablo Gomez, Vinutha Magal Shreenath, and Gabriele Meoni. Decentralised semi-supervised onboard learning for scene classification in low-earth orbit. *arXiv preprint arXiv:2305.04059*, 2023.
- [26] Ekin D Cubuk, Barret Zoph, Jonathon Shlens, and Quoc V Le. Randaugment: Practical automated data augmentation with a reduced search space. In *Proceedings of the IEEE/CVF conference on computer vision and pattern recognition workshops*, pages 702–703, 2020.
- [27] Mike Folk, Gerd Heber, Quincey Koziol, Elena Pourmal, and Dana Robinson. An overview of the hdf5 technology suite and its applications. In *Proceedings of the EDBT/ICDT 2011 workshop on array databases*, pages 36–47, 2011.
- [28] Mike Walmsley, Chris Lintott, Tobias Gérón, Sandor Kruk, Coleman Krawczyk, Kyle W Willett, Steven Bamford, Lee S Kelvin, Lucy Fortson, Yarin Gal, et al. Galaxy zoo decals: Detailed visual morphology measurements from volunteers and deep learning for 314 000 galaxies. *Monthly Notices of the Royal Astronomical Society*, 509(3): 3966–3988, 2022.
- [29] Oriol Vinyals, Charles Blundell, Timothy Lillicrap, Koray Kavukcuoglu, and Daan Wierstra. Matching networks for one shot learning. In *Advances in Neural Information Processing Systems (NeurIPS)*, volume 29, pages 3630–3638, 2016.

- [30] Avital Oliver, Augustus Odena, Colin A Raffel, Ekin Dogus Cubuk, and Ian Goodfellow. Realistic evaluation of deep semi-supervised learning algorithms. *Advances in neural information processing systems*, 31, 2018.
- [31] Eric Arazo, Diego Ortego, Paul Albert, Noel E O'Connor, and Kevin McGuinness. Pseudo-labeling and confirmation bias in deep semi-supervised learning. In *2020 International joint conference on neural networks (IJCNN)*, pages 1–8. IEEE, 2020.
- [32] Scott M Lundberg and Su-In Lee. A unified approach to interpreting model predictions. In I. Guyon, U. V. Luxburg, S. Bengio, H. Wallach, R. Fergus, S. Vishwanathan, and R. Garnett, editors, *Advances in Neural Information Processing Systems 30*, pages 4765–4774. Curran Associates, Inc., 2017. URL <http://papers.nips.cc/paper/7062-a-unified-approach-to-interpreting-model-predictions.pdf>.